Space- and time-resolved Seebeck and Nernst voltages in laser-heated permalloy/gold microstructures

Arndt von Bieren, Florian Brandl, Dirk Grundler, and Jean-Philippe Ansermet

Related Articles

Size-dependent transition of deformation mechanism, and nonlinear elasticity in Ni3Al nanowires
Appl. Phys. Lett. 102, 041902 (2013)

Local magnetization profile and geometry magnetization effects in microwires as determined by magneto-optical Kerr effect
J. Appl. Phys. 113, 043904 (2013)

Streak spectroscopy and velocimetry of electrically exploded Ni/Al laminates
J. Appl. Phys. 113, 043304 (2013)

Surface-enhanced Raman scattering from finite arrays of gold nano-patches
J. Appl. Phys. 113, 013103 (2013)

Magnetization reversal in graded anisotropy Co/Pt multilayers: A first order reversal curve study
J. Appl. Phys. 112, 123914 (2012)

Additional information on Appl. Phys. Lett.

Journal Homepage: http://apl.aip.org/

Journal Information: http://apl.aip.org/about/about_the_journal

Top downloads: http://apl.aip.org/features/most_downloaded

Information for Authors: http://apl.aip.org/authors

Space- and time-resolved Seebeck and Nernst voltages in laser-heated permalloy/gold microstructures

Arndt von Bieren,[1] Florian Brandl,[2] Dirk Grundler,[2,3] and Jean-Philippe Ansermet[1,a)]

[1]*Institute of Condensed Matter Physics, École Polytechnique Fédérale de Lausanne–EPFL, 1015 Lausanne, Switzerland*

[2]*Lehrstuhl für Physik funktionaler Schichtsysteme, Physik Department, Technische Universität München, James-Franck-Str. 1, 85748 Garching bei München, Germany*

[3]*Institute of Materials, École Polytechnique Fédérale de Lausanne–EPFL, 1015 Lausanne, Switzerland*

Thermoelectric effects in microstructured permalloy (Py)/Au wires are investigated using space- and time-resolved measurements based on scanning focused laser heating. Supported by numerical simulations of the temperature distribution, we identify two major contributions to the laser-induced signals: (i) the Seebeck effect due to thermocouples of Py/Au and (ii) the anomalous Nernst effect (ANE) in Py with a coefficient of $N_{ANE} \approx 1.6\,\mu V/K$. ANE-based magnetic imaging of magnetic domains and magnetization reversal is demonstrated with a lateral resolution on the μm scale. © 2013 American Institute of Physics. [http://dx.doi.org/10.1063/1.4789974]

Recent advancements in the field of spin caloritronics[1] have revealed effects arising from the interaction between spin and heat currents. A particularly intriguing example is the spin Seebeck effect[2–5] (SSE), originally observed in permalloy (Py)/platinum hybrid structures via the inverse spin-Hall effect. It describes the generation of a spin current when a ferromagnet (FM) is subjected to a temperature gradient. Here, the precise control of the temperature gradient is essential to identify and avoid spurious thermoelectric effects, in particular, in the transverse SSE configuration.[6–9]

Using laser-heating of a yttrium-iron garnet/platinum hybrid structure in the longitudinal SSE configuration, Weiler *et al.* reported spatially resolved measurements of both the anomalous Nernst effect (ANE) and the SSE.[10] In lateral FM/normal metal (NM) structures similar to the transverse SSE geometry, the effect of local temperature gradients have only been studied using Joule heating.[11] A detailed quantitative characterization of *laser-induced* temperature distributions and the resulting thermovoltages in FM/NM structures is lacking. A quantitative understanding is relevant however for spin caloritronics[1] and the recently reported thermoelectric detection of spin waves,[12] where an interplay of thermogalvanic and spin-related effects occurs.

In this letter, we study in detail laser-induced thermovoltages in lateral Py/Au wire structures. The choice of materials and film thicknesses excludes the SSE so as to focus on thermovoltages. Large Seebeck and ANE voltages are observed. Both effects are found to depend differently on the laser position and exhibit different time evolution, which can be accounted for by numerical modelling. We use the observed local character of the ANE to perform magnetic imaging on the μm length scale. Importantly, we show that time-dependent experiments are powerful to discriminate between the different thermovoltages.

Py wires, 4–10 μm wide and 22 nm thick, crossed by 2 pairs of 2 μm wide and 50 nm thick Au wires [Fig. 1(a)]

were prepared on single crystalline MgO substrates using a 2-step lift-off process and electron beam evaporation. Laser-heating experiments were conducted using a linearly polarized laser beam from either a solid state laser at $\lambda = 532\,nm$ or a laser diode (LD) (see Fig. 3(a)) at $\lambda = 660\,nm$. We focused the laser light by a microscope objective (Mitutoyo M Plan Apo, 20×) to a minimum spot size of $s \approx 2.6\,\mu m$ ($1/e^2$ intensity criterion) on the sample. The spot position was controlled using an *x*-*y*-*z* translation stage. Reflectivity and thermovoltage images were obtained by scanning the laser spot across the sample surface while simultaneously measuring the reflected intensity and the voltage drop between one pair of wires. We go beyond Weiler *et al.*[10] in that we perform both steady state and time-resolved readout of the thermovoltages. Finite element method (FEM)
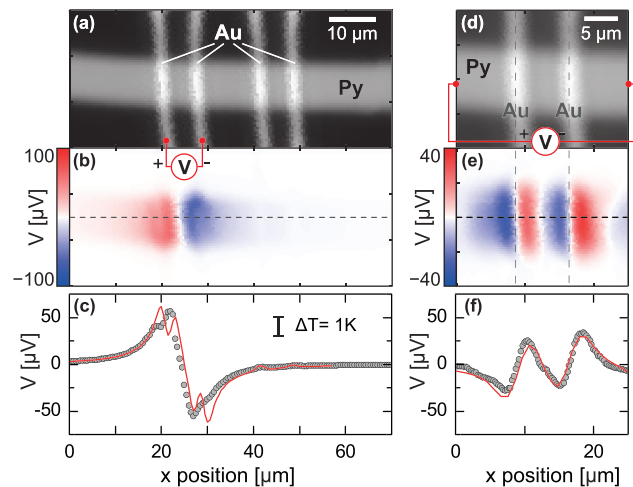

FIG. 1. Spatially resolved measurements of the Seebeck effect using scanning laser heating (spot size $s \approx 4\,\mu m$, laser power P $\approx 8\,mW$, $\lambda = 660\,nm$). (a) Reflectivity image of the structure. (b) Voltage measured between adjacent Au wires [as indicated in (a)] as a function of laser spot position. (c) Thermovoltage profile (circles: experimental data, solid line: simulation data) of Py wire along the dashed line shown in (b). (d) Reflectivity image and (e) and (f) thermovoltages (smaller scan area) when measuring the voltage drop along the Py wire [as indicated in (d)].

a)jean-philippe.ansermet@epfl.ch.

simulations of the laser-induced temperature distribution were performed using the COMSOL MULTIPHYSICS software package[13] with material parameters taken from the material database and Refs. 11 and 14.

First, we address the laser-induced voltages for zero magnetic field. Due to the different Seebeck coefficients of Py and Au ($S_{Au} = 1.7\,\mu V/K$, $S_{Py} = -20\,\mu V/K$),[11] each of the Py/Au interfaces forms a thermocouple (TC). Their common cold junction temperature T_c is given by the temperature of the bonding pads, which remains unaffected by the local laser heating. The voltage measured between any pair of Py/Au wires is therefore a direct measure of the average temperature rise of the corresponding Au/Py interface above room temperature. Figure 1(b) shows the thermovoltage measured between two adjacent Au wires as a function of laser spot position. The voltage reaches a local maximum/minimum (depending on the polarity of the TC) when directly heating one of the contacted TCs, indicating that the measured voltage in fact depends on the Py/Au interface temperature. Further confirmation is provided by the agreement between FEM simulations and experimental data for the line scan along the middle of the Py wire [Fig. 1(c)]. Here, the simulated average temperature rise of the TC interfaces is converted into a corresponding Seebeck voltage using $\Delta S = S_{Au} - S_{Py} = 21.7\,\mu V/K$. Remaining discrepancies are attributed to imperfections in the real sample geometry (rough edges) and a non-ideal laser beam profile (i.e., not purely Gaussian).

Slightly reduced Seebeck voltages occur when measuring the voltage drop along the Py wire [Figs. 1(d)–1(f)]. Due to differences in electrical conductivity, the Au layer dominates the effective Seebeck coefficient in regions where it covers the Py wire ($S_{eff} = (\sigma_{Au}S_{Au} + \sigma_{Py}S_{Py})/(\sigma_{Au} + \sigma_{Py}) \approx 0.26\,\mu V/K$). Hence, the configuration depicted in Fig. 1(d) can be approximated by an alternating series of wire sections with coefficients S_{Py} and S_{eff}. Temperature differences between left and right edges of the Au wire thus give rise to a Seebeck voltage, which results in the pattern shown in Fig. 1(e). The agreement between simulation data and experimental data [Fig. 1(f)] confirms this explanation.

Second, we address magnetization-dependent data. For this, we apply an in-plane magnetic field H as sketched in Fig. 2(a) and measure voltages V_x and V_y with and without a DC current I_{DC}. The magnetoresistance data shown in Fig. 2(b) are consistent with the anisotropic magnetoresistance (AMR) effect and indicate a reversal field of $H_c \approx 40\,Oe$ for the wire section between the inner Au wire pair [see Fig. 2(a)]. Magnetothermal voltages are measured for two fixed positions of the laser spot [see Fig. 2(a)]. Both spot positions are chosen such that the offset voltage due to the Seebeck effect [see Fig. 1] is minimized. Due to the presence of the substrate, the laser-generated temperature gradient ∇T has a strong component along z.

The magnetization-dependent voltage due to the ANE follows $\mathbf{E}_{ANE} = -N_{ANE}\,\mathbf{m} \times \nabla T$, with reduced magnetization $\mathbf{m} = \mathbf{M}/|\mathbf{M}|$ and Nernst coefficient N_{ANE}. When $\mathbf{m}$ is aligned with the wire, i.e., the x-direction, a voltage $V_{y,ANE} \propto m_x$ is generated along its width, as shown by the hysteresis loop in Fig. 2(c) for spot position (1). The voltage V_y follows an almost squared hysteresis loop with an abrupt variation near $|H_c| \approx 40\,Oe$.
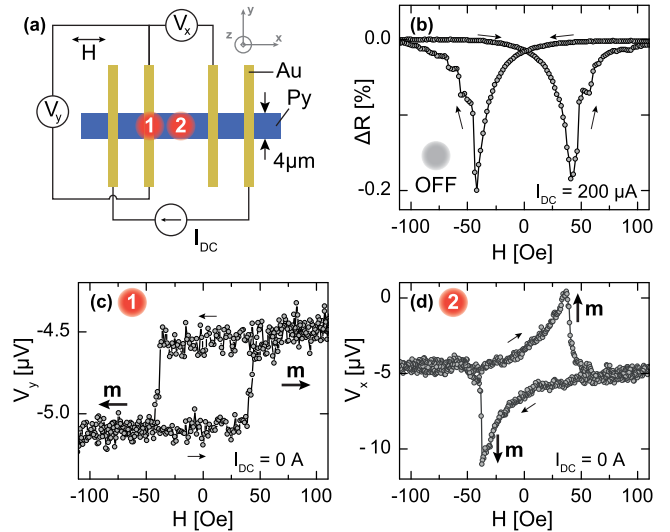

FIG. 2. AMR and ANE measured on a 4 μm wide Py wire using V_x and V_y. (a) Measurement geometry with laser spot positions used in (c) and (d) (spot size $s \approx 6\,\mu m$, $P \approx 11.7\,mW$, $\lambda = 532\,nm$). (b) $\Delta R = (R(H) - R(100\,Oe))/R(100\,Oe)$ in the absence of laser heating, derived from V_x measured at $I_{DC} = 200\,\mu A$ as a function of applied field H [$R(100\,Oe) = 128.9\,\Omega$], indicating magnetization reversal at $H_c \approx 40\,Oe$. (c) ANE signal $V_y \propto m_x$ and (d) $V_x \propto m_y$ as a function of H taken at $I_{DC} = 0$. Small black arrows indicate the sweep direction.

During magnetization reversal, $\mathbf{m}$ rotates and magnetic domains with non-zero m_y appear. This gives rise to a voltage $V_{x,ANE} \propto m_y$ along the wire. In Fig. 2(d), we observe field-dependent voltage signals for $0 \leq |H| \leq H_c$. Outside these intervals, i.e., $|H| > H_c$, the voltage V_x is nearly constant at $-5\,\mu V$. At $H \approx H_c$, the maximum voltage $V_{x,ANE}$ is observed, indicating a large m_y-component in the wire at the reversal field. The significant difference in peak-to-peak signal ($\Delta V_{x,ANE} \approx 11.5\,\mu V$ vs. $\Delta V_{y,ANE} \approx 0.55\,\mu V$) is attributed to the reduced heating power at position (1) due to a higher reflectivity of Au and the Au layer shunting the Py wire. The voltages V_x and V_y exhibit a remaining offset as the Seebeck voltage is small (compare Fig. 1) but not exactly zero.

Next, we demonstrate time-resolved measurements that are found to distinguish unequivocally Seebeck and Nernst voltages induced by laser heating. As shown in Fig. 3(a), the voltage is measured along x (along the Py wire) and across one Py/Au TC. A field of $|H| \approx 350\,Oe$ aligns $\mathbf{m}$ along $45°$ with respect to the wire axis. Laser pulses with a rise time of about 3 ns [at modulation frequency (TTL) $f = 10\,kHz$ with 50% duty cycle] locally heat the Py wire at a distance d from the Au wire. The resulting voltage is amplified and then recorded by a digital storage oscilloscope (nominal amplification factor is 20). Figure 3(b) shows the time-evolution of the amplified laser-induced voltage V_{amp} with respect to the rising edge of the laser pulse ($t = 0\,\mu s$) for $d = 4$, 10, and 15 μm and both field orientations $-H$ and $+H$. From the time-dependent signals, we extract two contributions with different time evolution: (i) a slowly growing increase, which dominates the overall voltage for small d and saturates for large t (on the order of 50 μs) and (ii) a fast-rising magnetization-dependent offset of constant magnitude. The $\mathbf{m}$-independent part $(V_{+H} + V_{-H})/2$ [Fig. 3(c)] varies significantly with increasing d: while the rise time increases (15.4 μs, 21.3 μs, and 25.8 μs), the overall signal strength
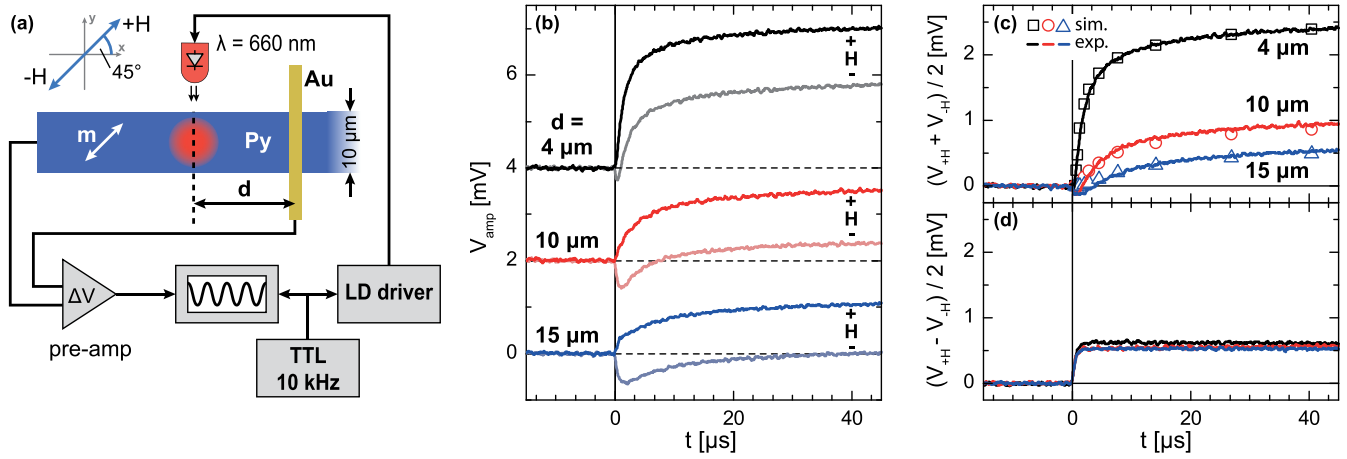
FIG. 3. Time-resolved measurement of ANE and Seebeck effect. (a) Measurement setup (spot size $s \approx 5.6\,\mu m$, $P_{peak} \approx 39.5\,mW$, $\lambda = 660\,nm$). (b) Voltage drop V_{amp} for $d = \{4, 10, 15\}\,\mu m$ for field orientations $+H$ and $-H$ [see (a)]. For clarity, the curves are offset by $2\,mV$. Field-independent (c) and field-dependent (d) part of the data shown in (b). Symbols in (c) show the simulated temperature rise at the Py/Au thermocouple (data are fitted to the experimental data using one common scaling factor).

decreases. This behavior is reproduced qualitatively by FEM simulations of the Seebeck voltages deduced from the rise of the temperature at the Py/Au interface [symbols in Fig. 3(c)], confirming the Seebeck effect as the origin of this position-dependent signal. The d-dependent rise time reflects the heat flow process between the laser spot and the TC.

In contrast to that, the **m**-dependent component ($V_{+H} - V_{-H}$)/2 [Fig. 3(d)] does not exhibit a significant dependence on d (as expected from the ANE) and shows a much faster rise time of $t_{rise} \approx 1.3\,\mu s$. As t_{rise} is setup-limited (the pre-amp bandwidth is 1 MHz), we assume the generation of the voltage to be instantaneous on the μs-timescale addressed here. We therefore conclude that the ANE voltage is locally generated at the position of the laser spot by the out-of-plane temperature gradient. These results highlight that the two effects can be unambiguously identified using time-resolved measurements.

The local character of the ANE signal now allows us to image magnetic domains on the μm scale. We use the configuration of Fig. 2(d) where the voltage is measured along the Py wire (i.e., $V_{x,ANE} \propto m_y$) [Fig. 4(a)]. The data are taken about $500\,\mu m$ away from the TCs to avoid Seebeck-induced voltages. The field is applied at an angle $\alpha \approx 45°$ [Fig. 4(b)]. The ANE voltage maps in Figs. 4(c) and 4(d) illustrate the spatial distribution of m_y for selected magnetic fields (scan size $50 \times 15\,\mu m^2$, step size 500 nm). In order to start from a homogeneously magnetized wire, the magnetization is "set" by applying a field of $|H| \approx 500\,Oe$ prior to recording images. In agreement with the direction of the applied field, a positive (negative) V_{ANE} indicates a positive (negative) component of **m** along y. This is confirmed by the top and bottom images in Figs. 4(c) and 4(d) that show uniformly magnetized states of the wire (indicated by black arrows). Assuming $\mathbf{m} \parallel \mathbf{H}$ at large $|H|$, we estimate the Nernst coefficient according to[10]

$$N_{ANE} \approx \frac{V_{ANE}}{\sin(\alpha)} \cdot \frac{w}{s^2\,\frac{\pi}{8}\,(\nabla_z T)_{max}},$$

with wire width $w = 10\,\mu m$ and spot size $s \approx 2.6\,\mu m$. $(\nabla_z T)_{max} \approx 17\,K/\mu m$ is the average out-of-plane temperature gradient at the center of the laser spot as deduced from

FEM simulations. The factor of $\pi/8$ arises from the approximation of the Gaussian distribution of $(\nabla_z T)$ by an equivalent square profile of width s. $V_{ANE} \approx 7.3\,\mu V$ is the maximum of the offset-corrected absolute voltage in the center of the wire. The factor $1/\sin(\alpha)$ accounts for the fact that
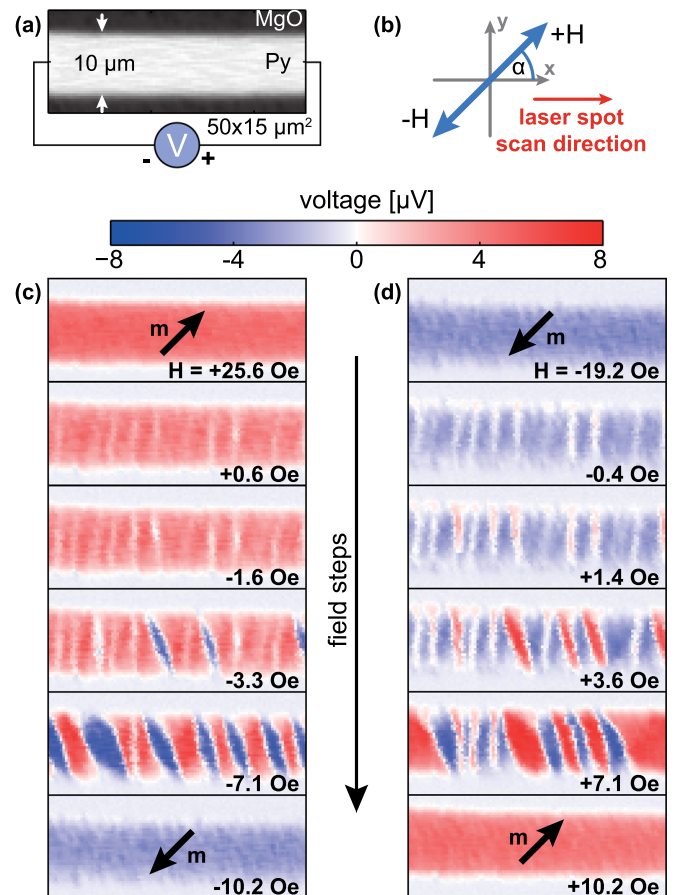

FIG. 4. ANE-based magnetic imaging of magnetization reversal in a $10\,\mu m$ wide Py wire (spot size $s \approx 2.6\,\mu m$, $P \approx 7.8\,mW$, $\lambda = 532\,nm$). (a) Reflectivity image ($50 \times 20\,\mu m^2$). V_{ANE} is measured along the Py wire as a function of laser spot position. (b) Field orientation ($\alpha \approx 45°$) and laser spot scan direction. (c) and (d) Sequence of V_{ANE} images with $V \propto m_y$ [see Fig. 2(c)] for both sweep directions of the magnetic field, illustrating the magnetization reversal.
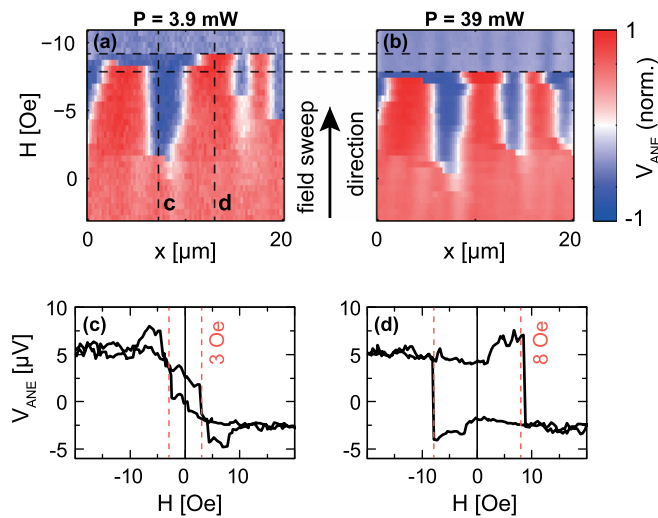
FIG. 5. (a) and (b) Field-dependent line scans: horizontal lines represent the ANE voltage as a function of laser spot position (scanned along the center of a Py wire) for different magnetic fields H (y-axis) close to the reversal field. (b) Same measurement with increased laser power. (c) and (d) Local hysteresis loops reflecting m_y measured at positions c and d indicated in (a).

only the voltage component along x is measured. We obtain a coefficient of $N_{ANE} \approx 1.6 \, \mu V/K$. This is close to what has been reported for Py ($2.6 \, \mu V/K$),[11] and significantly higher than the value for Ni ($0.06 \, \mu V/K$) reported in Ref. 10.

As expected for a $10 \, \mu m$ wide wire,[15] the magnetization reversal proceeds via the formation and growth of magnetic domains of reversed magnetization (see pronounced domain patterns at $\pm 7.1 \, Oe$). Interestingly, the patterns during the reversal process are found to be reproducible instead of randomly generated in each measurement. This is illustrated in Figs. 5(a) and 5(b), where we plot $20 \, \mu m$ long line-scans taken along the center of the Py wire as a function of magnetic field for two different heating powers ($P \approx 3.9 \, mW$ and $39 \, mW$). The x-positions where the reversed domains start to appear (blue regions) are consistently the same. The increased heating power, however, causes the reversal field to decrease by $1.3 \, Oe$ due to thermally assisted domain wall propagation and annihilation (see dashed horizontal lines). Local hysteresis loops are depicted in Figs. 5(c) and 5(d), which show V_{ANE} vs. H for two selected positions [indicated by vertical dashed lines in Fig. 5(a)]. The reversal fields of about $3 \, Oe$ and $8 \, Oe$ agree with the values in Fig. 5(a). We attribute the self-similar behavior of domain formation to imperfections in the shape of the wire, giving rise to nucleation sites and partial pinning of magnetic domains. Our results demonstrate that ANE-based magnetic imaging can be employed to analyze local details of the reversal mecha-nism on the μm scale. Focussing the laser down to the diffraction limit further enhances the spatial resolution. The technique is thus complementary to magneto-optical Kerr effect microscopy by which the functionality of Py nanowires for, e.g., racetrack-memory type devices has been studied.[16] Here, ANE-based microscopy is expected to be versatile by avoiding the polarization analysis of the reflected laser light.

In conclusion, we demonstrated that time-resolved measurements are key to identify and separate Seebeck and Nernst contributions to the thermovoltages in lateral Py/Au structures. Our results can be accounted for by numerical simulations of the temperature profiles obtained by laser-induced heating. Furthermore, magnetic imaging based on the anomalous Nernst effect was shown to be a viable imaging technique for the characterization of the magnetization structure on the μm length scale. The method is illustrated by analyzing the magnetic reversal behavior of a narrow Py wire.

[1]G. E. W. Bauer, E. Saitoh, and B. J. van Wees, Nature Mater. **11**, 391 (2012).
[2]K. Uchida, S. Takahashi, K. Harii, J. Ieda, W. Koshibae, K. Ando, S. Maekawa, and E. Saitoh, Nature **455**, 778 (2008).
[3]K. Uchida, J. Xiao, H. Adachi, J. Ohe, S. Takahashi, J. Ieda, T. Ota, Y. Kajiwara, H. Umezawa, H. Kawai, G. E. W. Bauer, S. Maekawa, and E. Saitoh, Nature Mater. **9**, 894 (2010).
[4]C. M. Jaworski, J. Yang, S. Mack, D. D. Awschalom, J. P. Heremans, and R. C. Myers, Nature Mater. **9**, 898 (2010).
[5]C. M. Jaworski, R. C. Myers, E. Johnston-Halperin, and J. P. Heremans, Nature **487**, 210 (2012).
[6]S. Y. Huang, W. G. Wang, S. F. Lee, J. Kwo, and C. L. Chien, Phys. Rev. Lett. **107**, 216604 (2011).
[7]S. Bosu, Y. Sakuraba, K. Uchida, K. Saito, W. Kobayashi, E. Saitoh, and K. Takanashi, J. Appl. Phys. **111**, 07B106 (2012).
[8]M. R. Sears and W. M. Saslow, Phys. Rev. B **85**, 035446 (2012).
[9]A. D. Avery, M. R. Pufall, and B. L. Zink, Phys. Rev. Lett. **109**, 196602 (2012).
[10]M. Weiler, M. Althammer, F. D. Czeschka, H. Huebl, M. S. Wagner, M. Opel, I.-M. Imort, G. Reiss, A. Thomas, R. Gross, and S. T. B. Goennenwein, Phys. Rev. Lett. **108**, 106602 (2012).
[11]A. Slachter, F. L. Bakker, and B. J. van Wees, Phys. Rev. B **84**, 020412 (2011).
[12]H. Schultheiss, J. E. Pearson, S. D. Bader, and A. Hoffmann, Phys. Rev. Lett. **109**, 237204 (2012).
[13]See www.comsol.com for COMSOL Multiphysics.
[14]E. D. Palik, *Handbook of Optical Constants of Solids* (Academic, 1998), Vol. 3.
[15]A. Hubert and R. Schäfer, *Magnetic Domains: The Analysis of Magnetic Microstructures* (Springer, 2008).
[16]P. Möhrke, T. A. Moore, M. Kläui, J. Boneberg, D. Backes, S. Krzyk, L. J. Heyderman, P. Leiderer, and U. Rüdiger, J. Phys. D: Appl. Phys. **41**, 164009 (2008).